metals

Article

# The Orowan Stress Measurement of Twinning Dislocations in Magnesium

**Xiao-Zhi Tang *** and **Ya-Fang Guo**

Institute of Engineering Mechanics, Beijing Jiaotong University, Beijing 100044, China; yfguo@bjtu.edu.cn
* Correspondence: xztang@bjtu.edu.cn; Tel.: +86-010-51687093

**Abstract:** The interaction between a lattice dislocation and non-shearable precipitates has been well explained by the Orowan bypass mechanism. The calculated additional shear stress facilitates the evaluation of precipitation hardening in metallic alloys. The lack of information about how a twinning dislocation behaves in the same scenario hinders our understanding of the strengthening against twin-mediated plasticity in magnesium alloys. In the current study, the bowing and bypassing of a twining dislocation impeded by impenetrable obstacles are captured by atomistic simulations. The Orowan stress measurement is realized by revealing the stick-slip dynamics of a twinning dislocation. The measured Orowan stress significantly deviate from what classic theory predicts. This deviation implies that the line tension approximation may generally overestimate the Orowan stress for twinning dislocations.

**Keywords:** twinning; interface defects; hardening; molecular dynamics; slip

check for updates

**Citation:** Tang, X.-Z.; Guo, Y.-F. The Orowan Stress Measurement of Twinning Dislocations in Magnesium. *Metals* **2021**, *11*, 1020. https://doi.org/10.3390/met11071020

Academic Editor: Eric Hug

Received: 20 May 2021
Accepted: 18 June 2021
Published: 24 June 2021



## 1. Introduction

During the past decades, the Orowan stress calculations based on the model developed by Bacon, Kocks and Scattergood (the BKS model) [1] were successful in the scenario of lattice dislocations (LDs) bypassing non-shearable precipitates in metallic alloys. The bowed-out LDs between precipitates before bypassing can be observed by experimental techniques such as transmission electron microscopy (TEM) [2–4] and simulation techniques such as molecular dynamics (MD) [5–7]. In lightweight, energy-efficient magnesium (Mg) alloys, the BKS model was also applied to calculate the Orowan stress needed by twinning dislocations (TDs), which are shear-driven line-defects and manipulate the behavior of a twin [8,9]. However, such an application meets problems.

The most remarkable problem is that there are no experiments nor simulations observing the bowing and bypassing of TDs in Mg alloys. Adding to the problem, the most profuse twins in Mg alloys ($\{10\bar{1}2\}$ extension twin) behave unconventionally [10–12], and its TD exhibits unique characters on the nucleation and propagation [13–16]. Because evaluating the strengthening against twins cannot be built on a hypothesis, the atomic-scale pictures of TD bowing and bypassing, especially the TD of the $\{10\bar{1}2\}$ extension twin, is imperative.

On the other hand, without such pictures, measuring the Orowan stress in mechanical testing experiments to see if the value matches the calculated one given by the BKS model can solve the problem disguisedly. Unfortunately, the Orowan stress is hard to measure in experiments because the back-stress exists in the strengthening against twins [17,18], and the back-stress cannot be precisely calculated due to the local plastic relaxation [17,19]. Therefore, although the total strengthening against twins can be measured [2,3,20,21], it is not known how much of the strengthening is due to the Orowan stress. Therefore, validating the numerical accuracy of the BKS model for TD needs other approaches than experimental means.

Over the past ten years, there have been lots of modifications to the BKS model, not for reflecting the differences between TD and LD, but for the complex behavior of a twin.

In 2011, Robson and collaborators used the standard BKS model to predict the Orowan stress when a $\{10\bar{1}2\}$ extension twin is impeded [18]. They found that the stress is an order of magnitude less than than that predicted on basal and prismatic LDs. This is due to the small Burgers vector of TD. In the next year, it was pointed out that there was no sufficient data for quantifying the actual magnitudes of both back-stress and Orowan stress [21]. In 2017, twins in magnesium were approximated by a super dislocation to give an equation calculating the Orowan stress needed for bowing the propagating twinning front between impenetrable particles [22]. This equation was adopted for qualitative analysis in 2020 to support the bias effects on twin growth and twin nucleation by basal precipitate plates in a Mg–Al alloy [2]. In 2018, Robson and Barnett pointed out in a review that an equivalent simple equation to the BKS model predicting the strengthening effect of precipitates against twins would be very useful, but the physical basis for such an equation remains unclear [17]. In 2019, an Orowan precipitate hardening equation specifically applicable to twin propagation was developed [23]. A scenario of TDs piling-up and bowing at a line of non-shearable obstacles was adopted to modify the BKS model of Orowan stress calculation by the TD number, $n$. In the same year, the effective planar interparticle spacing $\overline{L}$ and the mean planar diameter of the particles on the twinning plane $\overline{D}$ in the BKS model were also adjusted according to experimental results [20]. All these modifications gradually constructed an integrated theoretical framework for calculating the Orowan stress of twin-precipitate interaction. However, as mentioned, all of them regarded a TD as an LD. Since a TD is structurally, energetically and thus dynamically different from an LD [8], their line tension deserves a cautious differentiation.

In this article, we adopted MD simulations to offer a clear picture of a single TD bowing out between impenetrable obstacles and to measure the Orowan stress by monitoring the critical resolved shear stress (CRSS) change of TD gliding. These two goals are achieved for the first time to our best knowledge.

## 2. Materials and Methods

A system containing a preset dipole of TD lines on a coherent twin boundary (CTB) is established as Figure 1 shows. The simulation cell has periodic boundary conditions (PBC) along the x- and z-directions. Thus, there are two free surfaces parallel to the CTB. The TD of $\{10\bar{1}2\}$ extension twinning ($\mathbf{TD^E}$) is primarily studied as well as the TD of $\{10\bar{1}1\}$ compression twinning ($\mathbf{TD^C}$) for a comparison. The TD dipole is driven by the shear strain of the system. First, the two TDs glide freely in opposite directions as the two white arrows indicate in Figure 1. Consequently, the CRSS of TD glide $\tau_g$ ($\tau_g^{\mathbf{E}}$ for $\mathbf{TD^E}$ and $\tau_g^{\mathbf{C}}$ for $\mathbf{TD^C}$) can be measured. To be noted, $\tau_g$ is different from the CRSS of CTB migration $\tau_m$. $\tau_m$ normally refers to the stress needed for the homogeneous nucleation of TD, while $\tau_g$ has a comparable meaning to the Peierls–Nabarro stress of an LD. Second, a pair of thin, cylindrical, impenetrable obstacles are placed in front of the TDs. The TD–obstacle distances *P1* and *P2* are different for lowering down the probability that two TDs meet their own obstacles at the same time. Due to the PBC along the z-direction, the TDs will equivalently meet a line of collinear obstacles and bow out between them. The same scenario was used to establish the BKS model [1]. Thus, in this standard way, the Orowan stress ($\tau_O$) of TD is measured in the current simulations.

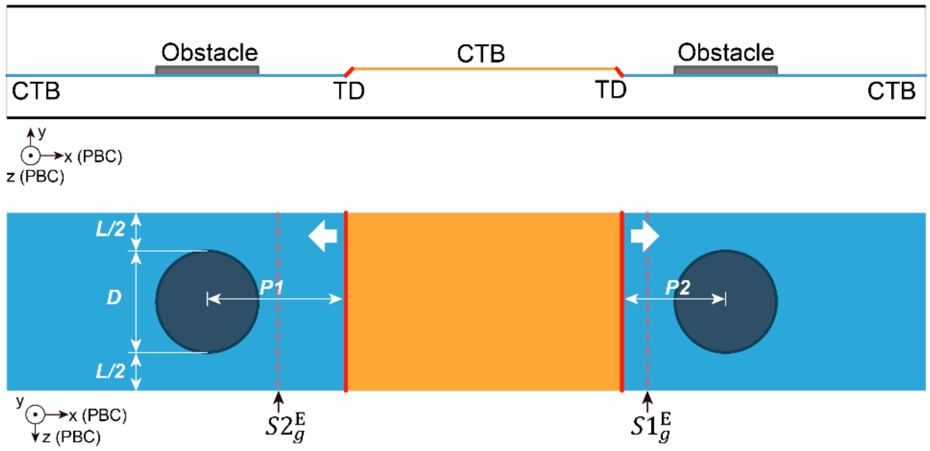


**Figure 1.** The schematic diagram of the simulation system containing a CTB and a TD dipole. The two black cylinders are the impenetrable obstacles used for Orowan stress measurement.

## 3. Results

$\tau_g$ is measured at 5 K. Low thermal fluctuations make it almost impossible for the two TDs to glide simultaneously. Thus, what we observed in repeated simulations is that once a TD glides, the other TD stays stationary. Such behavior is convenient for CRSS measurement. The strain rate adopted is $2 \times 10^6$ s$^{-1}$. This strain rate is not too computationally expensive but is still low enough that the stick-slip dynamics of a TD may recover. The observed stick-slip behavior is reflected by the saw-tooth time dependencies of RSS in Figure 2. In a stick event, the RSS linearly increases, and a TD is quiescent. In a slip event, the RSS drops, and the TD glides to a new position (different positions corresponding to different slip events for $\mathbf{TD^E}$ are denoted in Figure 1). Peak RSS values separating the two events are $\tau_g$. $\tau_g$ varies according to the number of kink pairs on a TD line when the TD glides. If there is only one kink pair (it facilitates the glide by repeated nucleation and annihilation), the CRSS is low (slip event $S1_g^E$). If there are multiple kink pairs operating at the same time, the CRSS is high (slip events $S2_g^E$ and $S3_g^E$). The kinks captured during $S1_g^E$ and $S2_g^E$ are shown in Figure 2. Since the occurrence of multiple kinks is a basic dislocation motion mechanism and there has to be multiple kinks when a TD is bowed, $\tau_g^E$ is considered as 51 MPa. For $\mathbf{TD^C}$, only a multiple-kink case is observed at this rate and temperature, so $\tau_g^C$ is 53 MPa (Figure 2).

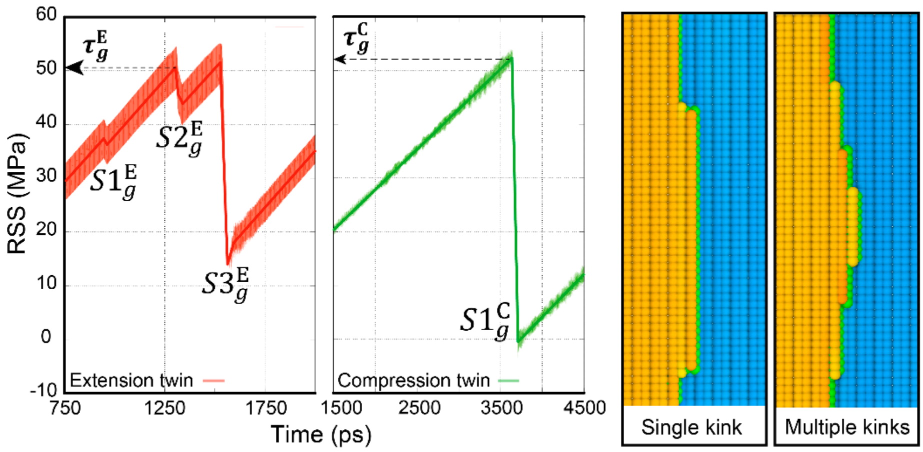


**Figure 2.** On the left is the stick-slip behaviors separately of two TDs reflected by the time dependencies of RSS. The measured RSS data are made translucent, and the solid lines are smoothed data after noise filtering. On the right are the captured kink pairs on a TD line.

When the impenetrable obstacles shown in Figure 1 are placed in front of the TDs, the peak RSS value raises due to the TD pinning at the obstacle. From the pinning starts to the pinning ends, the TDs are observed to bow out between obstacles and finally bypass them (Figure 3). At the low temperature and strain rate we adopted, the whole pinning process is accomplished by several stick and slip events. That is to say, the bowing-out configuration stays unchanged for most of the time. This phenomenon can clearly reveal the CRSS to overcome the impediment on TD by obstacles. Therefore, the highest peak RSS among those pinning-related slip events minus $\tau_g$ equals $\tau_O$. For $\mathbf{TD^E}$, one of the TDs starts to glide in $S1_O^E$ as Figure 2(a2) shows and stops at the configuration that Figure 3(a3) shows. In $S2_O^E$, the other TD glides. Thus, this bowing configuration that Figure 3(a3) shows does not change until $S3_O^E$ starts. In $S3_O^E$, the other TD, which is not shown, stays stationary. The peak RSS of $S1_O^E$ is significantly higher than $\tau_g^E$ because there are more kink pairs on the TD line (comparing to $S2_g^E$ in Figure 1c), and the obstacle induces local stress field, which impedes the TD before it glides. The peak RSS of $S3_O^E$ is due to overcoming the TD pinning, and it is 69 MPa. Therefore 69 MPa minus $\tau_g^E$ equals 18 MPa, the $\tau_O^E$ (note that precipitate size $D$ is 6 nm). For $\mathbf{TD^C}$, in $S2_O^C$, one of the TDs starts to glide as Figure 3(b2) shows and stops at the configuration that Figure 3(b3) shows. This bowing configuration does not change until $S5_O^C$ starts. Therefore $\tau_O^C$ is obtained as 15 MPa (note that $D$ is 5 nm).

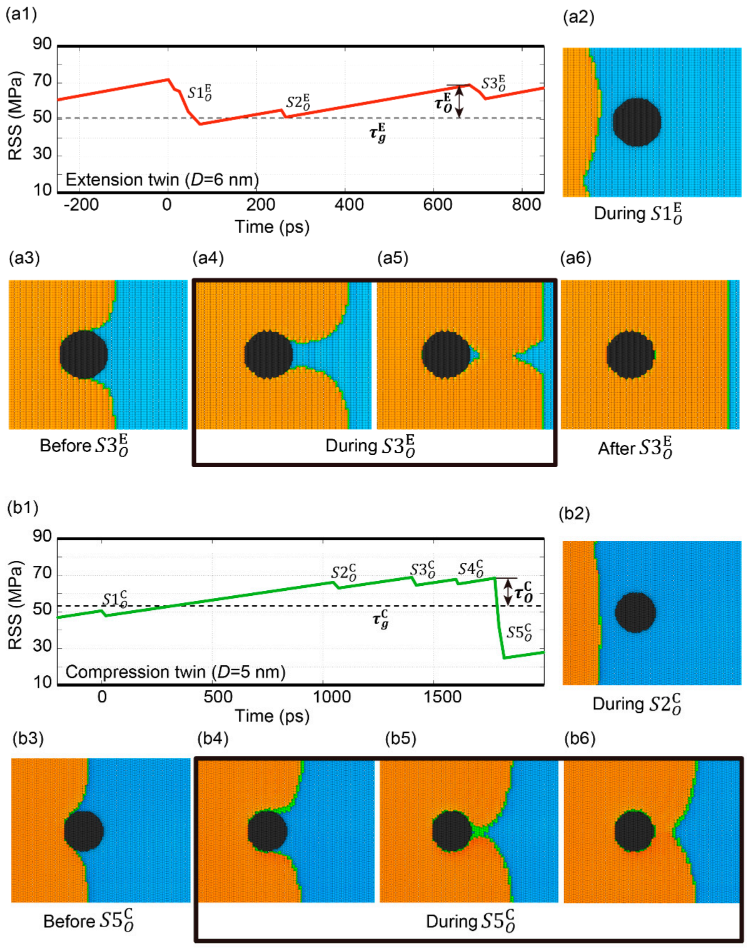


**Figure 3.** (**a1**,**b1**) The stick and slip events separately for extension twin and compression twin. Raw data of RSS are not shown. In the atomic-scale pictures of TD bowing and bypassing captured in MD simulation for extension twin (**a2**–**a6**) and compression twin (**b2**–**b6**), atoms are colored by their coordinates along the y-direction: orange for migrated CTB, blue for original CTB, and green for partially migrated CTB. Black ones compose the obstacles.

## 4. Discussion

In the simulations, the cell dimension along the z-direction ($D$ plus precipitate spacing $L$) is kept the same. $D$ is changed so the Orowan stress as the function of $D$ can be measured, and it is plotted separately for $\mathbf{TD^E}$ and $\mathbf{TD^C}$ in Figure 4a,b. The theoretical value of Orowan stress is also plotted as a comparison to find out the difference between a TD and LD. The equation of Orowan stress in standard BKS model is

$$\boldsymbol{\tau_O} = K\frac{Gb}{L}\ln\left(\frac{2\overline{D}}{b}\right) \tag{1}$$

where $K$ is $1/2\pi$ or $1/2\pi(1-\mu)$ for edge or screw, respectively, ($\mu$ is the Poisson's ratio, and to be noted, the edge and screw components are not exactly the same as they are in a TD; the detailed difference need further investigation), $G$ is the shear modules of the twinned system, $b$ is the magnitude of the Burgers vector, and $\overline{D}$ is the harmonic mean of precipitate size $D$ and spacing $L$ ($\overline{D} = \left(D^{-1}+L^{-1}\right)^{-1}$). For the $\{10\bar{1}2\}$ extension twin, $G$ is measured to be 21.24 GPa in current simulations, and $b$ is 0.049 nm for $\mathbf{TD^E}$ [24]. For the $\{10\bar{1}1\}$ compression twin, $G$ is measured to be 6.928 GPa in current simulations, and $b$ is 0.173 nm for $\mathbf{TD^C}$ [25]. To be noted, the $\mathbf{TD^C}$ constructed here is the two-layer one (($\boldsymbol{b}$, $2h_0$) TD) [25], which has both the edge and screw components [26]. In Figure 4, it can be seen that both $\mathbf{TD^E}$ and $\mathbf{TD^C}$ have a much lower measure of Orowan stress than theoretically calculated. An apparent gentle modification of Equation (1) is a coefficient that proportionally reduces the calculated value, so the Orowan stress specifically for TD is $A \times \boldsymbol{\tau_O}$. After the data fitting, the coefficient $A$ is 0.297 for $\mathbf{TD^E}$ and 0.136 for $\mathbf{TD^C}$. The fitted lines are plotted in the figure. Another modification is to let $\boldsymbol{\tau_O} - B$ be the Orowan stress for TD. After the data fitting, the coefficient $B$ is 45.5 MPa for $\mathbf{TD^E}$ and 83.1 MPa for $\mathbf{TD^C}$. The fitted lines can also be seen in the figure. $A$ and $B$ represent different ways of regarding the difference between a TD and an LD. $A$ means this TD–LD difference changes with the geometric factors of obstacle, such as $D$ (actually, it is $\overline{D}$ taking the effect). If $D$ is much smaller than $L$, this TD–LD difference can be ignored. $B$ means the TD–LD difference does not change. If the size, shape and distribution of precipitates are all the same, replacing LDs in metals with TDs always gets the same reduction on RSS. It can be noticed that, for both $\mathbf{TD^E}$ and $\mathbf{TD^C}$, the measured Orowan stress drops significantly as $D$ decreases. When $D$ is 4 nm, there is no Orowan stress for $\mathbf{TD^E}$ because the stress needed for bypassing is lower than the one needed for gliding $\boldsymbol{\tau_g^E}$. For $\mathbf{TD^C}$, it is also quite small (<5 MPa). The second modification ($\boldsymbol{\tau_O} - B$) gives a better fitting on this downtrend. Therefore, although $\boldsymbol{\tau_O} - B$ is not a perfect modification, we still prefer it. Either way, the results demonstrate that comparing with a LD, dropping conventional line tension approximation does overestimate the Orowan stress for a TD. Few studies particularly focused on the line tension of a TD in magnesium, but at least the arbitrary shape of $\mathbf{TD^E}$ loop when CTB migrates implies its weak line tension [13,15].

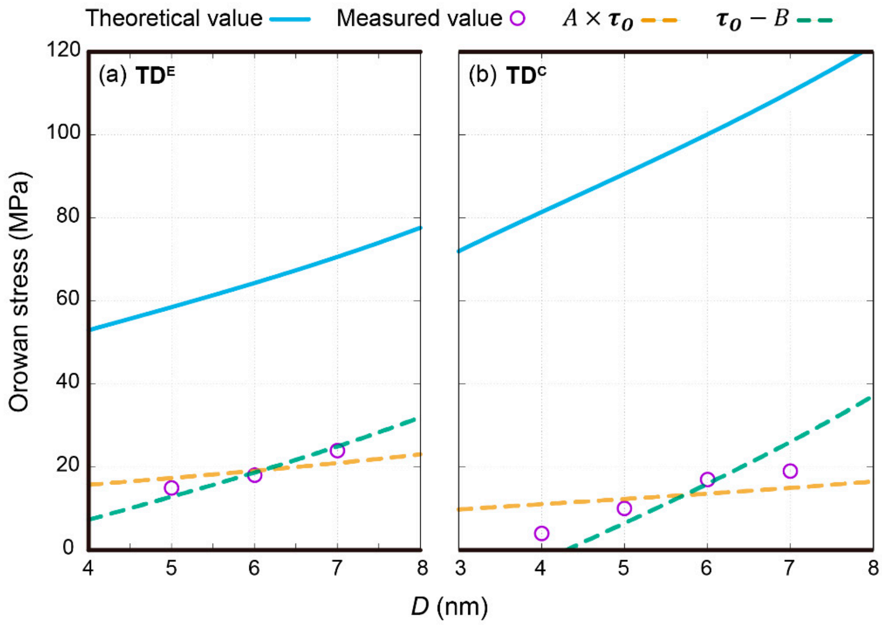


**Figure 4.** The comparison between theoretical values given by the equation of BKS model, measured values, and modified values of Orowan stress for TD of (**a**) $\{10\bar{1}2\}$ extension twin and (**b**) $\{10\bar{1}1\}$ compression twin.

## 5. Conclusions

In conclusion, the measurement of the Orowan stress on twinning dislocation in magnesium is achieved in MD simulations to verify the applicability of conventional BKS equation in twin-precipitate interaction. Results show that for the two representative twins in magnesium (the $\{10\bar{1}2\}$ extension twin and the $\{10\bar{1}1\}$ compression twin), the twinning dislocations have much weaker line tension (≈60% for extension twin and ≈80% for compression twin) than the lattice dislocations with the same magnitudes of Burgers vectors do. The corresponding Orowan stress is significantly lower than what BKS equation gives. In this case, the twinning dislocations in magnesium are supposed to barely contribute to the precipitation hardening, leaving only the back-stress dominating. This might be why the size, shape, and volume fraction of the precipitates are more important than their effective spacing in the design of high-strength Mg alloys [10].

It is worth mentioning that twinning dislocation is not the only shear-driven line-defect that the classic BKS model fails to precisely treat. The Orowan stress of the pyramidal dislocation in Mg alloys [2], and of the LDs in Al–Mg–Si alloys [27], cannot be well predicted by the BKS model either. High-throughput atomistic simulations might help in establishing a connection between the atomic core structure/energy of line-defects and their line tension, and by then, a universal Orowan law for precipitation hardening in crystalline materials can be expected.

**Author Contributions:** Conceptualization, methodology, software, validation, formal analysis, investigation, resources, data curation, writing—original draft preparation, project administration, funding acquisition, X.-Z.T.; writing—review and editing, Y.-F.G. All authors have read and agreed to the published version of the manuscript.

**Funding:** This work was supported by the National Natural Science Foundation of China (Nos. 11972071).

**Institutional Review Board Statement:** Not applicable.

**Informed Consent Statement:** Not applicable.

**Conflicts of Interest:** The authors declare no conflict of interest.

## References


1. Bacon, D.; Kocks, U.; Scattergood, R. The effect of dislocation self-interaction on the Orowan stress. *Philos. Mag.* **1973**, *28*, 1241–1263. [CrossRef]
2. Ma, X.; Jiao, Q.; Kecskes, L.J.; El-Awady, J.A.; Weihs, T.P. Effect of basal precipitates on extension twinning and pyramidal slip: A micro-mechanical and electron microscopy study of a Mg–Al binary alloy. *Acta Mater.* **2020**, *189*, 35–46. [CrossRef]
3. Wang, C.; Cepeda-Jiménez, C.M.; Pérez-Prado, M.T. Dislocation-particle interactions in magnesium alloys. *Acta Mater.* **2020**, *194*, 190–206. [CrossRef]
4. Alizadeh, R.; LLorca, J. Interactions between basal dislocations and $\beta 1'$ precipitates in Mg–4Zn alloy: Mechanisms and strengthening. *Acta Mater.* **2020**, *186*, 475–486. [CrossRef]
5. Liao, M.; Li, B.; Horstemeyer, M. Interaction Between Basal Slip and a $Mg_{17}Al_{12}$ Precipitate in Magnesium. *Metall. Mater. Trans. A* **2014**, *45*, 3661–3669. [CrossRef]
6. Vaid, A.; Guénolé, J.; Prakash, A.; Korte-Kerzel, S.; Bitzek, E. Atomistic simulations of basal dislocations in Mg interacting with $Mg_{17}Al_{12}$ precipitates. *Materialia* **2019**, *7*, 100355. [CrossRef]
7. Esteban-Manzanares, G.; Alizadeh, R.; Papadimitriou, I.; Dickel, D.; Barrett, C.; LLorca, J. Atomistic simulations of the interaction of basal dislocations with $MgZn_2$ precipitates in Mg alloys. *Mater. Sci. Eng. A* **2020**, *788*, 139555. [CrossRef]
8. Hirth, J.P.; Wang, J.; Tomé, C.N. Disconnections and other defects associated with twin interfaces. *Prog. Mater. Sci.* **2016**, *83*, 417–471. [CrossRef]
9. He, Y.; Li, B.; Wang, C.; Mao, S.X. Direct observation of dual-step twinning nucleation in hexagonal close-packed crystals. *Nat. Commun.* **2020**, *11*, 1–8. [CrossRef]
10. Liu, B.-Y.; Yang, N.; Wang, J.; Barnett, M.; Xin, Y.-C.; Wu, D.; Xin, R.-L.; Li, B.; Narayan, R.L.; Nie, J.-F.; et al. Insight from in situ microscopy into which precipitate morphology can enable high strength in magnesium alloys. *J. Mater. Sci. Technol.* **2018**, *34*, 1061–1066. [CrossRef]
11. Zhang, X.Y.; Li, B.; Wu, X.L.; Zhu, Y.T.; Ma, Q.; Liu, Q.; Wang, P.T.; Horstemeyer, M.F. Twin boundaries showing very large deviations from the twinning plane. *Scr. Mater.* **2012**, *67*, 862–865. [CrossRef]
12. Tang, X.-Z.; Guo, Y.-F. The engulfment of precipitate by extension twinning in Mg–Al alloy. *Scr. Mater.* **2020**, *188*, 195–199. [CrossRef]
13. Spearot, D.E.; Capolungo, L.; Tomé, C.N. Shear-driven motion of Mg $\{10\bar{1}2\}$ twin boundaries via disconnection terrace nucleation, growth, and coalescence. *Phys. Rev. Mater.* **2019**, *3*, 53606. [CrossRef]
14. Sato, Y.; Swinburne, T.; Ogata, S.; Rodney, D. Anharmonic effect on the thermally activated migration of $\{10\bar{1}2\}$ twin interfaces in magnesium. *Mater. Res. Lett.* **2021**, *9*, 231–238. [CrossRef]
15. Tang, X.-Z.; Zu, Q.; Guo, Y.-F. The diffusive character of extension twin boundary migration in magnesium. *Materialia* **2018**, *2*, 208–213. [CrossRef]
16. Luque, A.; Ghazisaeidi, M.; Curtin, W.A. A new mechanism for twin growth in Mg alloys. *Acta Mater.* **2014**, *81*, 442–456. [CrossRef]
17. Robson, J.D.; Barnett, M.R. The effect of precipitates on twinning in magnesium alloys. *Adv. Eng. Mater.* **2019**, *21*, 1800460. [CrossRef]
18. Robson, J.D.; Stanford, N.; Barnett, M.R. Effect of precipitate shape on slip and twinning in magnesium alloys. *Acta Mater.* **2011**, *59*, 1945–1956. [CrossRef]
19. Fan, H.; Zhu, Y.; El-Awady, J.A.; Raabe, D. Precipitation hardening effects on extension twinning in magnesium alloys. *Int. J. Plast.* **2018**, *106*, 186–202. [CrossRef]
20. Hidalgo-Manrique, P.; Robson, J.D. Interaction Between Precipitate Basal Plates and Tensile Twins in Magnesium Alloys. *Metall. Mat. Trans. A* **2019**, *50*, 3855–3867. [CrossRef]
21. Stanford, N.; Geng, J.; Chun, Y.B.; Davies, C.H.J.; Nie, J.F.; Barnett, M.R. Effect of plate-shaped particle distributions on the deformation behaviour of magnesium alloy AZ91 in tension and compression. *Acta Mater.* **2012**, *60*, 218–228. [CrossRef]
22. Barnett, M.R. Twinning Super Dislocations to Help Understand Strength. In Proceedings of the International Conference on Martensitic Transformations, Chicago, IL, USA, 9–15 July 2017; pp. 143–145.
23. Barnett, M.R.; Wang, H.; Guo, T. An Orowan precipitate strengthening equation for mechanical twinning in Mg. *Int. J. Plast.* **2019**, *112*, 108–122. [CrossRef]
24. Wang, J.; Hoagland, R.G.; Hirth, J.P.; Capolungo, L.; Beyerlein, I.J.; Tomé, C.N. Nucleation of a $(\bar{1}012)$ twin in hexagonal close-packed crystals. *Scr. Mater.* **2009**, *61*, 903–906. [CrossRef]
25. Wang, J.; Beyerlein, I.J.; Hirth, J.P.; Tome, C.N. Twinning dislocations on $\{\bar{1}011\}$ and $\{\bar{1}013\}$ planes in hexagonal close-packed crystals. *Acta Mater.* **2011**, *59*, 3990–4001. [CrossRef]
26. Zu, Q.; Tang, X.-Z.; Fu, H.; Peng, Q.-M.; Guo, Y.-F. The irrational shear of $\{10\bar{1}1\}$ twinning in Mg. *Materialia* **2019**, *5*, 100239. [CrossRef]
27. Hu, Y.; Curtin, W.A. Modeling peak-aged precipitate strengthening in Al–Mg–Si alloys. *J. Mech. Phys. Solids* **2021**, *151*, 104378. [CrossRef]